Reduced order modeling and suboptimal control of a solid fuel ignition model

MICHAEL HINZE[1] & ANDREAS KAUFFMANN[2]

PREPRINT NO. 636/1999

[1]Technische Universität Berlin, Fachbereich Mathematik, Straße des 17. Juni 136, D-10623 Berlin & Karl-Franzens Universität Graz, Institut für Mathematik, Heinrichstr. 36, A-8010 Österreich, email: hinze@math.tu-berlin.de

[2]Technische Universität Berlin, Fachbereich Mathematik, Straße des 17. Juni 136, D-10623 Berlin, email: kauffman@math.tu-berlin.de

Abstract

The snapshot form of the proper orthogonal decomposition is used to compute approximate solutions and to develop suboptimal open- and closed-loop control strategies for the perturbed Gelfand equation. The behaviour of the reduced system is investigated numerically wrt perturbations of the external heating and the initial values. In the control part of this note several suboptimal control approaches using the reduced dynamics are discussed. In particular the performance of a simple feedback control law is numerically validated against the solution of the full optimal control problem.

Contents

1 Introduction **4**

2 The instationary perturbed Gelfand equation **5**

3 Proper orthogonal decomposition with snapshots **6**

4 Proper orthogonal decomposition applied to the perturbed Gelfand equation **7**

4.1 Mode generation for the perturbed Gelfand equation 7

4.2 Numerical solution of the perturbed Gelfand equation using proper orthogonal decomposition 9

4.2.1 Homogeneous initial value 10

4.2.2 Discontinuous, but symmetric initial value 10

4.2.3 Discontinuous and unsymmetric initial value 11

4.2.4 Symmetric and asymmetric external heating 11

4.2.5 First conclusions 13

4.2.6 Enlargement of the proper orthogonal decomposition basis 14

5 Optimization using proper orthogonal decomposition **16**

5.1 A table steered feedback controller 19

5.2 Table gouverned control for (OCP_y) 20

5.3 Discussion of table controllers 22

5.4 Proper orthogonal decomposition for storage intensive problems 23

6 Conclusions **24**

7 Epilogue: On the sense of numerical testing **25**

1 Introduction

The computation of optimal control policies for physical systems gouverned by time dependent nonlinear partial differential equations is not always possible with todays available computing facilities, see e.g. [5]. This may be due to insufficient computing power or, limited storage, or to both. These restrictions naturally lead to suboptimal control concepts whose philosophie consists in providing good controls with reasonable computational effort rather than optimal controls. In the recent past several suboptimal control concepts have been developed and have been applied to a great variety of control problems, e.g. [1, 5, 6, 7, 12, 10] and the references cited therein.

In the present note we discuss suboptimal control approaches based on the reduction of the underlying partial differential equation by use of the snapshot form of the proper orthogonal decomposition (POD) introduced by Sirovich in [11]. All numerical tests are carried out at hand of the nonlinear perturbed Gelfand equation (PGE), which models the ignition process in solid fuels.

2 The instationary perturbed Gelfand equation

Let $\Omega \subset \mathbb{R}^n$ be a bounded domain.

The instationary perturbed Gelfand equation (PGE) is given by

$$y_t - \Delta y = \delta \exp\left(\frac{y}{1+\varepsilon y}\right), \qquad y|_{t=0} = y_0, \quad y|_{\partial\Omega} = 0, \quad t > 0, \tag{1}$$

with parameters δ and ε satisfying $\delta > 0$ and $0 < \varepsilon \ll 1$.

Similar to the instationary Gelfand equation

$$y_t - \Delta y = \delta e^y, \qquad y|_{t=0} = y_0, \quad y|_{\partial\Omega} = 0, \quad t > 0, \tag{2}$$

the perturbed Gelfand equation is obtained from asymptotic expansion of the solid fuel ignition model

$$\begin{array}{rcl} T_t - \Delta T &=& \varepsilon\delta\mu^m \exp\left(\frac{T-1}{\varepsilon T}\right), \qquad T|_{t=0} = 1, \qquad T|_{\partial\Omega} = 1, \\ \mu_t - \beta\Delta\mu &=& -\varepsilon\delta\Gamma\mu^m \exp\left(\frac{T-1}{\varepsilon T}\right), \qquad \mu|_{t=0} = 1, \qquad \frac{\partial}{\partial n}\mu\big|_{\partial\Omega} = 0, \end{array} \tag{3}$$

which for $t > 0$ describes the dynamics of the temperature T and the mass μ of a chemical species in thermal reaction processes. Here, $\beta \geq 0$, $\delta, \Gamma, \varepsilon > 0$ and ε^{-1} denotes activation energy.

The behaviour of the solutions of (2) depends on n, δ, Ω and y_0. For the case of $y_0 \equiv 0$ there are two possibilities. Either there exist solutions of the stationary problem and the solution of (2) converges to one of them or there is no solution of the stationary equation and a blowup occurs, i.e. there is a time $T \in (0, \infty)$ and a point $x \in \Omega$ such that $\lim_{t \to T} y(t, x) = \infty$. This may be interpreted as an explosive thermal event. If there are solutions of the stationary problem it depends on y_0 whether the solution converges to one of them or a blowup occurs.

In contrast solutions to (1) do not blow up since the stationary equation always possesses solutions whose number depends on n, ε, δ and Ω. If there are exactly three solutions, as is the case for Ω equal to the unit Ball in $\mathbb{R}^2$ the small one and the large one are stable, and the solution in between is unstable. However, for certain parameter constellations the scale of the small solution compared to that of the large solution is minor and thus, a solution may look "blowup-like", as it has to grow very fast to reach the large solution.

A more detailed discussion of of equations (2), (1) and of the model (3) can be found in [3].

3 Proper orthogonal decomposition with snapshots

Applying the standard techniques to the space discretization of partial differential equations like the one given in (1) results in large-dimensional systems of ODEs. Having in mind the numerical solution of optimization problems with the discretized partial differential equation serving as subsidiary condition, large system dimension clearly is a drawback. One possibility to overcome this drawback is to construct low-dimensional systems containing an appropriate amount of the dynamics and to use them as subsidiary conditions instead. One possibility of constructing low-order models is the snapshot proper orthogonal decomposition approach developed by Sirovich in [11] which we describe next.

Suppose M snapshots $\{y_k := y(t_k) : 1 \leq k \leq M\}$ of the solution of the partial differential equation at time instances $0 \leq t_1 < \cdots < t_M$ are given. It then follows from interpolation theory that the larger M, i.e. the finer the time grid, the more system dynamics is represented by the space $Y_M := \operatorname{span}\{y_k := y(t_k) : 1 \leq k \leq M\}$. The basic idea of the POD method now consists in constructing a suitable orthogonal basis of this space with the help of the eigenvectors and eigenvalues of the correlation matrix $K = (k_{kl})$ whose entries are given by

$$k_{kl} = \int_\Omega y_k y_l \, dx = \langle y_k,\, y_l \rangle_{L^2(\Omega)}\,, \qquad (1 \leq k, l \leq M). \tag{4}$$

Clearly, K is positive semidefinite and therefore, has real, nonnegative eigenvalues λ_j associated to eigenvectors v^j. The POD basis functions (in what follows also referred to as POD modes) then are given by

$$\varphi_i = \sum_{k=1}^{M} v_k^i y_k. \tag{5}$$

We note that it is not hard to show that these modes are pairwise orthogonal. Due to the construction of the modes no N-dimensional subset ($N \leq M$) of the space Y_M contains more information wrt the L^2 scalar product than $\Phi_N = \{\varphi_i : 1 \leq i \leq N\}$, $N \leq M$, see also [2, 9, 1]. In order to obtain a low-dimensional basis for a Galerkin Ansatz modes corresponding to small eigenvalues are neglected. One possible smallness-criterion can be given in terms of the relative *information content* I of the base, which is defined by

$$\mathrm{I}(N) := \sum_{k=1}^{N} \lambda_k / \sum_{k=1}^{M} \lambda_k.$$

If a basis is required that contains 78% of the total information contained in the space Y_M, say the dimension N of the subspace Φ_N is determined by

$$\mathrm{N} = \operatorname{argmin} \left\{ \mathrm{I}(N); \mathrm{I}(N) \geq \frac{78}{100} \right\}$$

The use of the normalized snapshots $y_k = \frac{y(t_k)}{\|y(t_k)\|}$ instead of $y_k = y(t_k)$ allows for a statistical interpretation of the POD method as principal component analysis applied to the given data. In [9] the POD approach is put into the more general frame of singular value decomposition.

4 Proper orthogonal decomposition applied to the perturbed Gelfand equation

We now give a brief on how to construct modes and low-dimensional dynamical systems with the help of the proper orthogonal decomposition approach.

4.1 Mode generation for the perturbed Gelfand equation

First, we construct POD modes for our model problem (1), using $\Omega = (-1, +1) \subset \mathbb{R}^1$, $\delta = 1$, $\varepsilon = 0.175$ and $y_0 = 5\cos(\pi x/2)$. For this purpose due to the dynamical properties of the PGE snapshots are taken in the

initial phase, the transient phase and the fully developed phase, see Fig. 1 where 6 snapshots are shown. The eigenvalues of the correlation matrix K in (4) are given by $\lambda_1 = 8.78 \cdot 10^{+05}$, $\lambda_2 = 1.63 \cdot 10^{+01}$, $\lambda_3 = 9.36 \cdot 10^{-02}$, $\lambda_4 = 1.58 \cdot 10^{-04}$, $\lambda_5 = 4.41 \cdot 10^{-06}$, and $\lambda_6 = 1.24 \cdot 10^{-09}$, the corresponding modes are shown in Fig. 2. As one can see nearly the total energy contained in the set Y_6 is resembled in the first mode.
These are the modes used in all of the tests described below.

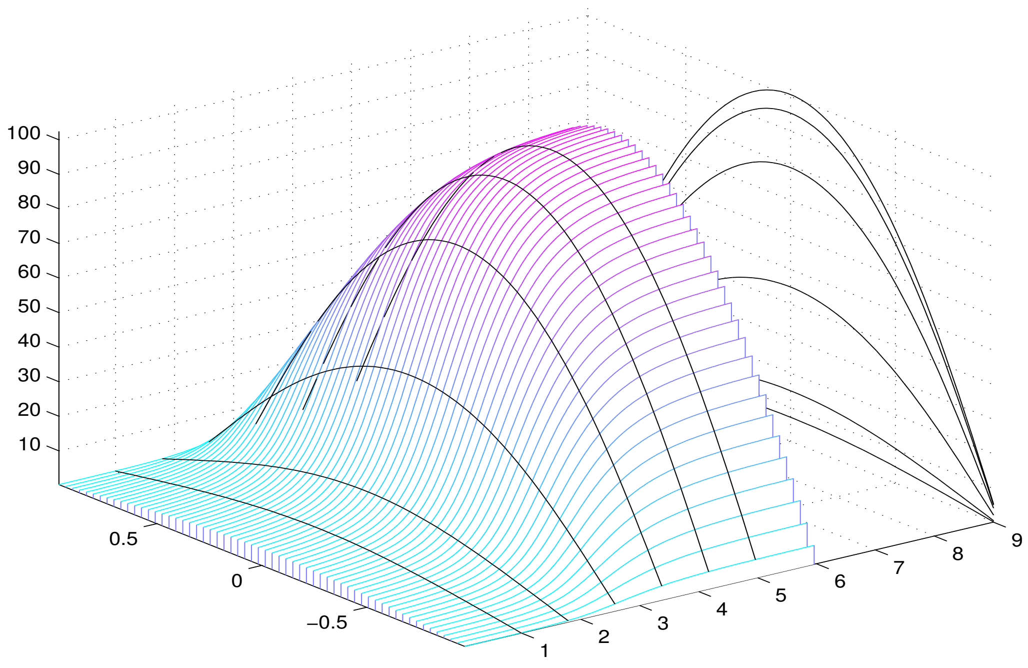

Figure 1: Solution of PGE and snapshots

The results for the Ansatz $y_k = \frac{y(t_k)}{\|y(t_k)\|}$ are similar. The modes have almost the same shape, with very little differences in the height and location of the extrema only. This is also the case for modes generated from snapshots of the solution to the initial value $y_0 = 0$, which converges to the small stable steady state of the equation. This indicates self-similarity of the solution of PGE wrt time. However, we have to mention, that these differences become more significant for parameters ε smaller than $\varepsilon_0 = 0.1$.

We need to mention that for the numerical computation of the snapshots 60 grid points are used for the spatial discretization of the PGE (1), which corresponds to a space grid spacing of $\partial x \approx 0.033$. For the numerical integration of the resulting system of ordinary differential equations

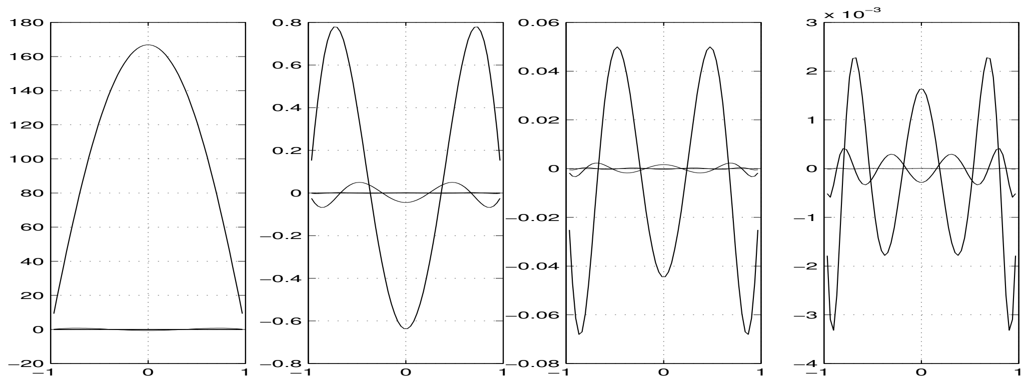

Figure 2: Modes

$y_t + Ly = h(y) + u$ the semi implicit Euler method

$$(I + \partial t \cdot L)\, y(t + \partial t) = Iy(t) + \partial t \cdot (h(y(t)) + u(t + \partial t))\,. \tag{6}$$

with fixed stepsize $\partial t \approx 0.04$ is used.

4.2 Numerical solution of the perturbed Gelfand equation using proper orthogonal decomposition

First we test the ability of the Galerkin Ansatz using POD modes as Ansatz functions to approximate the solution of the PGE for different starting values y_0 and perturbations u of the right hand side, which later will play the role of a distributed control. Inserting

$$y_N := \sum_{j=1}^{N} a_j \varphi_j \tag{7}$$

into eq. (1) and testing with mode φ_i we obtain the ODE system

$$\langle \varphi_i, \varphi_i \rangle \, \dot{a}_i + \sum_{j=1}^{N} \underbrace{\langle \nabla\varphi_j, \nabla\varphi_i \rangle}_{=:\, d_{ij}} a_i = \underbrace{\left\langle \delta \exp\left(\frac{\sum a_j \varphi_j}{1 + \varepsilon \sum a_j \varphi_j} \right), \, \varphi_i \right\rangle}_{=:\, g_i(a)} + \underbrace{\langle u, \varphi_i \rangle}_{=:\, b_i}, \tag{8}$$

or more briefly

$$\dot{a} + Da = g(a) + b, \qquad a|_{t=0} = a_0, \tag{9}$$

with $a_{0i} := \langle y_0, \varphi_i \rangle$ and $\langle \cdot, \cdot \rangle$ denoting the $L^2(\Omega)$-scalar product.

4.2.1 Homogeneous initial value

We use $u \equiv 0$ and $y_0 \equiv 0$. For that configuration the solution converges to the small stable steady state of PGE. N denotes the number of modes. In all tables that follow we use the abbreviations

$$|y - y(a)|_{abs} := \|y - y(a)\|_{L^\infty(Q)} \text{ and } |y - y(a)|_{rel} := \left\| \frac{y - y(a)}{y} \right\|_{L^\infty(Q)},$$

where $Q = (t_0, T) \times \Omega$ is a time-space cylinder, y denotes the state computed from the full system and $y(a)$ for a computed from (9) is given by (7). Since we do not expect the POD predictions to be very good in the initial phase we present data with respect to the time intervals $[0, 9]$ and $[1, 9]$.
In Tab. 1 the numerical simulation of the PGE for different number of modes are shown. The solutions for $N = 3$ are depicted in Fig. 3.

	$0 \le t \le 9$		$1 \le t \le 9$		
	$\|y - y(a)\|_{abs}$	$\|y - y(a)\|_{rel}$	$\|y - y(a)\|_{abs}$	$\|y - y(a)\|_{rel}$	Flops
$N = 2$	0.003674	0.276309	0.003674	0.044755	267 751
$N = 3$	0.000993	0.135144	0.000984	0.021269	340 201
$N = 4$	0.000467	0.071853	0.000467	0.011241	196 201

Table 1: POD simulations for $y_0 = 0$ and no external heating u

Solving numerically the original equation needs 257 400 Flops. Thus, using POD does not reduce the computational costs. This is caused by the evaluation of the non-linearity $g(a)$, which has to be carried out in the large-dimensional finite element space. If the spatial domain Ω is chosen as a subset in a higher dimensional space the relative numerical expenses decrease.

4.2.2 Discontinuous, but symmetric initial value

Again we use $u \equiv 0$, but now a symmetric, discontinuous initial value

$$y_0 = c \cdot \begin{cases} 1 & x \in (-1, -1/2) \\ 1/2 & x \in [-1/2, +1/2] \\ 1 & x \in (+1/2, +1), \end{cases}$$

where c denotes a real constant.

As one can see in Tab. 2 for the POD system for times greater than 0 resolves the dynamics of the full system very good. The situation becomes slightly more worse in the case of unsymmetric initial values y_0 for the full system, see Tab. 3.

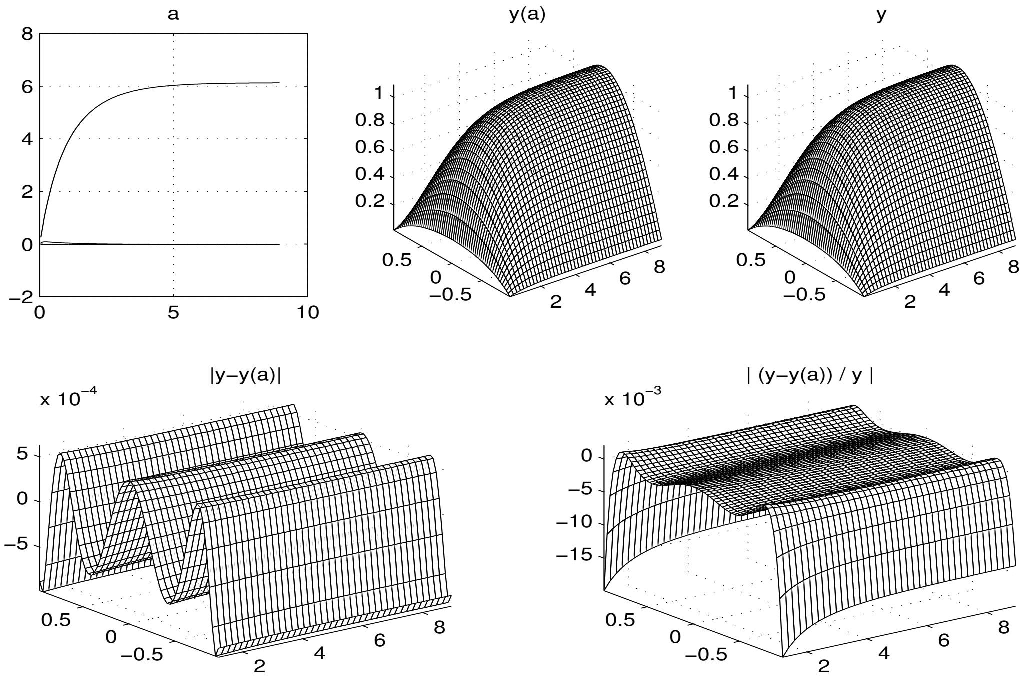

Figure 3: Solution of PGE and POD prediction: $N = 3$, $y_0 = 0$, $u = 0$

4.2.3 Discontinuous and unsymmetric initial value

Again we set $u \equiv 0$. The initial value

$$y_0 = c \cdot \begin{cases} 1 & x \in (-1, 0) \\ 1/2 & x \in [0, +1) \end{cases}$$

is unsymmetric. c again denotes a real constant.

In the case of $c = 10$ the POD simulations predict the beginning of the transient phase to late which causes retarded dynamics and explains the large error in this case.

Next we present some numerical tests with vanishing initial value and some external heating.

4.2.4 Symmetric and asymmetric external heating

We set $y_0 \equiv 0$ and fix the number of modes as $N = 3$. A plot of the dynamics of the POD system is given in Fig. 4 and the numerical comparison for this example is presented in Tab. 4.

	$0 \leq t \leq 9$		$1 \leq t \leq 9$	
$N=2$	$\lvert y-y(a)\rvert_{abs}$	$\lvert y-y(a)\rvert_{rel}$	$\lvert y-y(a)\rvert_{abs}$	$\lvert y-y(a)\rvert_{rel}$
c=1	0.064374	0.264275	0.003676	0.036150
c=10	0.673505	0.263931	0.209092	0.009285
c=100	6.380155	0.263464	0.083120	0.001741
$N=3$	$\lvert y-y(a)\rvert_{abs}$	$\lvert y-y(a)\rvert_{rel}$	$\lvert y-y(a)\rvert_{abs}$	$\lvert y-y(a)\rvert_{rel}$
c=1	0.021142	0.119063	0.000966	0.015479
c=10	0.239263	0.117802	0.026744	0.001634
c=100	2.054326	0.121216	0.007914	0.000170
$N=4$	$\lvert y-y(a)\rvert_{abs}$	$\lvert y-y(a)\rvert_{rel}$	$\lvert y-y(a)\rvert_{abs}$	$\lvert y-y(a)\rvert_{rel}$
c=1	0.021953	0.102351	0.000471	0.008363
c=10	0.248793	0.104503	0.033387	0.001081
c=100	2.054141	0.102800	0.011360	0.000119

Table 2: POD simulations for discontinuous, symmetric initial value y_0, no external heating u

	$0 \leq t \leq 9$		$1 \leq t \leq 9$	
$N=2$	$\lvert y-y(a)\rvert_{abs}$	$\lvert y-y(a)\rvert_{rel}$	$\lvert y-y(a)\rvert_{abs}$	$\lvert y-y(a)\rvert_{rel}$
c=1	0.461070	9.060953	0.006391	0.042201
c=10	8.262197	32.389255	8.262197	0.236130
c=100	49.864560	48.833627	2.311873	0.028134
$N=3$	$\lvert y-y(a)\rvert_{abs}$	$\lvert y-y(a)\rvert_{rel}$	$\lvert y-y(a)\rvert_{abs}$	$\lvert y-y(a)\rvert_{rel}$
c=1	0.449392	10.113335	0.003975	0.020959
c=10	8.326771	38.537885	8.326771	0.232051
c=100	47.186640	58.600620	2.329992	0.028522
$N=4$	$\lvert y-y(a)\rvert_{abs}$	$\lvert y-y(a)\rvert_{rel}$	$\lvert y-y(a)\rvert_{abs}$	$\lvert y-y(a)\rvert_{rel}$
c=1	0.444540	10.513280	0.003885	0.013245
c=10	8.350215	41.401793	8.350215	0.232084
c=100	47.664365	63.019820	2.335531	0.028548

Table 3: POD simulations for discontinuous, unsymmetric initial value y_0, no external heating u

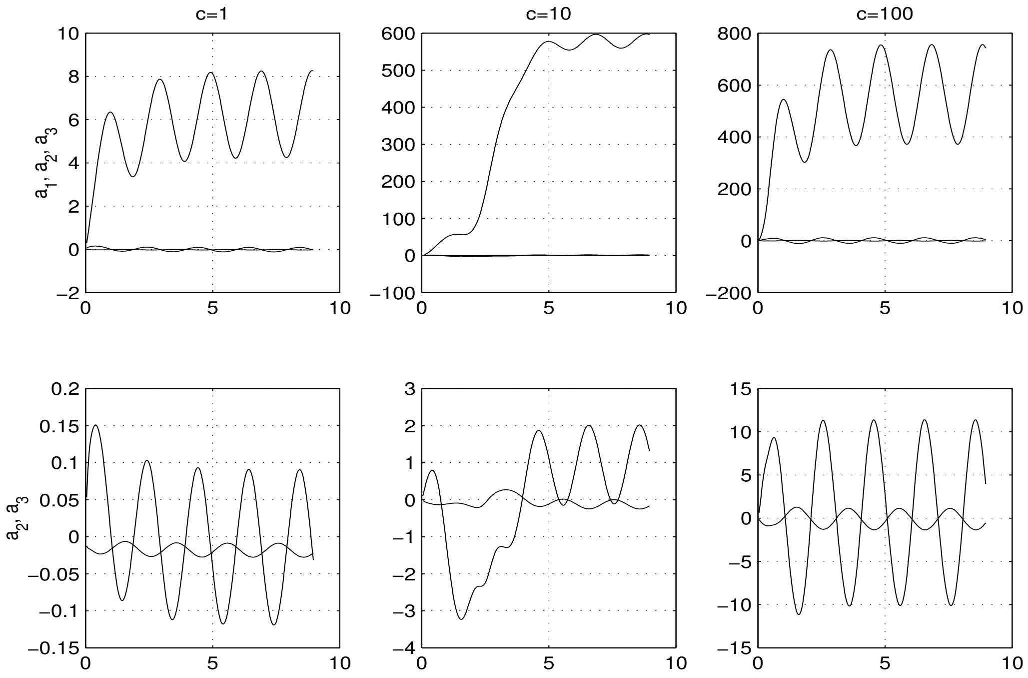

Figure 4: Dynamic of modes for $u = c \cdot \sin \pi t$, $y_0 = 0$

4.2.5 First conclusions

The POD method performs very good in predicting the solution of the PGE. Problems arise, of course, if the POD approach based on symmetric snapshots only is used to approximate unsymmetric solutions. To overcome this problem unsymmetric snapshots should be generated and taken into account for the computation of the POD modes.

Another error source arises from the POD approximation a_0 of the initial value y_0, since the beginning of the transient phase of the PGE is very sensitive wrt perturbations. Moreover, although the PGE seems to be quite robust along its stable solutions it behaves very sensitive in the transient area between them, as is well demonstrated in Tab. 3 for the case $c = 10$.

We mention that tests leading to $y_a(t,x) = \sum a_j(t)\varphi_j(x) < -\varepsilon^{-1}$ for some (t,x) should be avoided. We encountered this phenomenon in numerical experiments with

$$y_0 = c \cdot \begin{cases} 1 & x \in (-1, -1/2) \\ 0 & x \in [-1/2, +1/2] \\ 1 & x \in (+1/2, +1) \end{cases}$$

and $u = 0$ for some sufficiently large $c \in \mathbb{R}$. It also occurred for y and $\sum a_j \varphi_j$ in the last test presented in Tab. 4 for $c = 10$ instead of $c = 20$.

$u = c \cdot \sin \pi t$	$0 \le t \le 9$		$1 \le t \le 9$	
	$\|y - y(a)\|_{abs}$	$\|y - y(a)\|_{rel}$	$\|y - y(a)\|_{abs}$	$\|y - y(a)\|_{rel}$
c=1	0.001972	0.135144	0.001950	0.027964
c=10	0.013527	0.135144	0.013527	0.022396
c=100	0.103885	0.135144	0.103885	0.029172
$u = c \cdot \sin \pi t \cdot \chi_{\{x<0\}}(x)$				
c=1	0.068842	0.234884	0.068842	0.224856
c=20	7.933665	2.549729	7.933665	0.531670
c=100	9.270626	7.320827	7.555080	0.436912

Table 4: POD simulations $y_0 = 0$, symmetric and asymmetric external heating

The behaviour of the modes is depicted in Figs. 3 and 4. The dominance of the first mode is typical. It describes the dynamics inherent in the system nearly completely. We will exploit this fact later for generation of a simple feedback controller.

4.2.6 Enlargement of the proper orthogonal decomposition basis

As is demonstrated in the previous sections modes generated from a specific data set are limited in their application. In order to improve the behaviour of the corresponding dynamical POD system there are a lot of ways to enrich the snapshot set or the set of modes. If, for example unsymmetry has to be introduced to the simulations one may add a "pseudo snapshot" to our snapshot set or a "pseudo mode" (orthogonal to the POD modes) to the POD basis. Extending the previous numerical experiments we introduce the additional "information"

$$\psi(x) = \chi_{\{x<0\}}(x) = \begin{cases} 1 & x \in (-1, 0) \\ 0 & x \in [0, 1) \end{cases} \tag{10}$$

as pseudo snapshot and as pseudo mode, respectively to the system. The results are shown in Tabs. 5, 6 (pseudo snapshot) and Tab. 7 (pseudo mode).

Although the bases all are different (see Fig. 5) no differences in the quality of the numerical predictions are visible in the tables. This seems to indicate that the POD method best reflects the dynamics inherent in the data sample, no matter how these samples are arranged. In other words,

$y_0 = c \cdot \chi_{\{x<0\}}(x)$ $u = 0$	$0 \le t \le 9$ $\lvert y - y(a)\rvert_{abs}$	 $\lvert y - y(a)\rvert_{rel}$	$1 \le t \le 9$ $\lvert y - y(a)\rvert_{abs}$	 $\lvert y - y(a)\rvert_{rel}$
c=1	0.351374	6.498187	0.002328	0.019079
c=10	4.412232	22.748902	4.412232	0.131894
c=100	37.684602	31.750868	1.451613	0.018390
$y_0 = 0$ $u = c \cdot \sin \pi t \cdot \chi_{\{x<0\}}(x)$				
c=1	0.064589	0.196889	0.064589	0.191136
c=20	7.809603	1.933761	7.809603	0.351971
c=100	8.779532	5.075142	7.075307	0.320395

Table 5: Results for adding ψ to the snapshot set and using 4 modes

$y_0 = c \cdot \chi_{\{x<0\}}(x)$ $u = 0$	$0 \le t \le 9$ $\lvert y - y(a)\rvert_{abs}$	 $\lvert y - y(a)\rvert_{rel}$	$1 \le t \le 9$ $\lvert y - y(a)\rvert_{abs}$	 $\lvert y - y(a)\rvert_{rel}$
c=1	0.351374	6.498189	0.002328	0.019079
c=10	4.412230	22.748835	4.412230	0.131894
c=100	37.684598	31.750757	1.451613	0.018390
$y_0 = 0$ $u = c \cdot \sin \pi t \cdot \chi_{\{x<0\}}(x)$				
c=1	0.064589	0.196889	0.064589	0.191136
c=20	7.809603	1.933760	7.809603	0.351971
c=100	8.779531	5.075138	7.075308	0.320395

Table 6: Results for adding $100 \cdot \psi$ to the snapshot set and using 4 modes

$y_0 = c \cdot \chi_{\{x<0\}}(x)$ $u = 0$	$0 \le t \le 9$ $\lvert y - y(a)\rvert_{abs}$	 $\lvert y - y(a)\rvert_{rel}$	$1 \le t \le 9$ $\lvert y - y(a)\rvert_{abs}$	 $\lvert y - y(a)\rvert_{rel}$
c=1	0.351375	6.498165	0.002328	0.019077
c=10	4.412229	22.748502	4.412229	0.131894
c=100	37.684635	31.750247	1.451613	0.018390
$y_0 = 0$ $u = c \cdot \sin \pi t \cdot \chi_{\{x<0\}}(x)$				
c=1	0.064589	0.196889	0.064589	0.191137
c=20	7.809606	1.933751	7.809606	0.351970
c=100	8.779535	5.075102	7.075301	0.320396

Table 7: Results for adding an orthonormalization of ψ to the POD base of 3 modes

POD is the best filter for the dynamics contained in a data sample, such as a set of snapshots of a dynamical system.

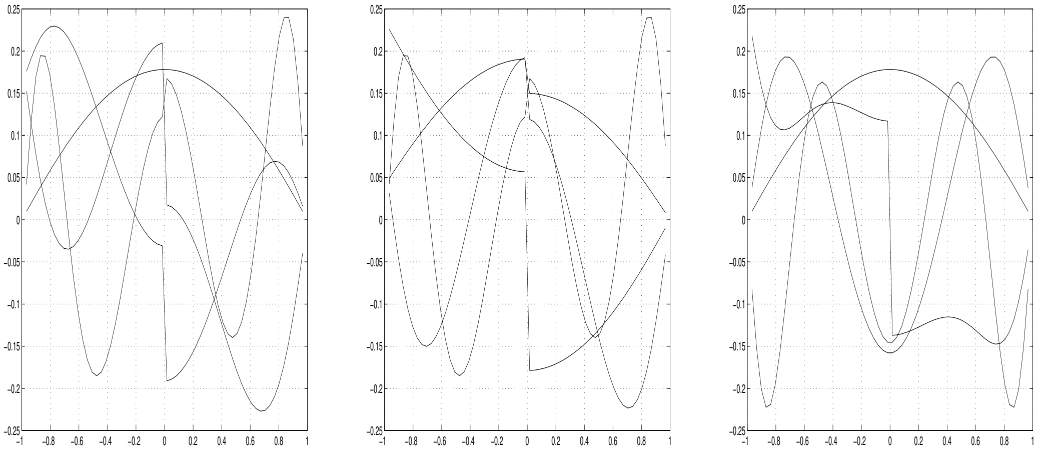

Figure 5: Enlarged function bases; From left to the right: adding ψ to the snapshot set, adding $100 \cdot \psi$ to the snapshot set, adding orthonormal part of ψ to the mode set

5 Optimization using proper orthogonal decomposition

Once snapshots of a dynamical system are available one can try to use them for computing suboptimal controls of the original system. In order present some possibilities we consider the optimal control problem (OCP_y) :

$$(\mathrm{OCP}_y) \begin{cases} \min J(y,u) \\ \text{s.t.} \\ y_t - \Delta y = \delta \exp\left(\frac{y}{1+\varepsilon y}\right) + u, \quad y|_{t=0} = y_0, \quad y|_{\partial\Omega} = 0, \quad t > 0, \\ y \geq -\varepsilon^{-1}, \end{cases} \tag{11}$$

where

$$J(y,u) := \int_0^T \tfrac{1}{2}\|y(t) - y_d\|^2_{L^2(\Omega)} + \tfrac{\nu}{2}\|u(t)\|^2_{L^2(\Omega)}\,dt \tag{12}$$

is a cost functional of tracking type and y_d shall be a time independent observation.

In what follows we will not treat the inequality constraint $y \geq -\varepsilon^{-1}$ explicitly.

With a Galerkin Ansatz using POD modes we may transform (OCP_y) into the low dimensional problem (OCP_a) :

$$(\mathrm{OCP}_a) \begin{cases} \min J(a,b) \\ \text{s.t.} \\ a_t - Da = g(a) + b, \quad a|_{t=0} = a_0, \quad t > 0 \\ \sum a_j \varphi_j \geq -\varepsilon^{-1} \end{cases} \tag{13}$$

with

$$J(a,b) := \int_0^T \tfrac{1}{2}\|a(t) - a_d\|^2_{\mathbb{R}^N} + \tfrac{\nu}{2}\|b(t)\|^2_{\mathbb{R}^N}\, dt, \tag{14}$$

and $a_{0i} := \langle y_0, \varphi_i \rangle$ and $a_{di} := \langle y_d, \varphi_i \rangle$.
If the number of modes N is small and thus the dimension of system in (13) using SQP methods (OCP_a) can be solved at low numerical costs. At each SQP step we have to solve the system

$$\left(\begin{array}{cc|c} H(a,\lambda) & & P(a)^T \\ & \nu I & -I \\ \hline P(a) & -I & \end{array}\right) \begin{pmatrix} \partial a \\ \partial b \\ \partial \lambda \end{pmatrix} + \begin{pmatrix} P(a)^T\lambda + a - a_d \\ \nu b - \lambda \\ a_t - Da - g(a) - b \end{pmatrix} = 0, \tag{15}$$

where $P(a) := \partial_t - D - g'(a)$ and $H(a,\lambda) := I - g''(a)^T\lambda$.

To solve (15) we compute $\partial\lambda$ using the Schur complement

$$\Big(\underbrace{P(a)H(a,\lambda)^{-1}P(a)^T + \tfrac{1}{\nu}I}_{=:\, O_{SC}}\Big)\partial\lambda = r_1, \tag{16}$$

where

$$r_1 = a_t - Da - g(a) - b - P(a)H(a,\lambda)^{-1}(P(a)^T\lambda + a - a_d) - b + \tfrac{1}{\nu}\lambda. \tag{17}$$

With $\partial\lambda$ available it is easy to compute ∂a and ∂b from

$$\partial b = \tfrac{1}{\nu}(\partial\lambda - \nu b + \lambda) \quad \text{and} \tag{18}$$

$$P(a)\partial a = \partial b - a_t + Da + g(a) + b. \tag{19}$$

The most expensive part in this process is the evaluation of $g'(a)$ and $g''(a)\lambda$, since scalar products have to be evaluated in the high dimensional

	(OCP_y)	(OCP_a)
evaluation of first order information	389 461	235 058
construction of second order operator	228 606	1 001 038
solving of second order system	461 689 690	163 773
one SQP step	463 061 651	1 651 568
complete optimization (for $y_d = 150 \cdot \psi$)	1 852 569 853	11 554 641

Table 8: Comparison of Matlab Flops

finite element space. Let m be the number of steps in time, n the number of finite elements and N the number of modes. Then computation of $g'(a)$ and $g''(a)\lambda$ amounts to $O(m \cdot n \cdot N^2)$ flops. Once $g'(a)$ and $g''(a)\lambda$ are available solving for $\partial\lambda$ in (16) and ∂a in (19) amounts to $O(m \cdot N^3)$ flops when the semi-implicit Euler scheme (6) is used. This is quite neglectable for $N \ll n$. In the following tests we used $m = 225$, $n = 60$ and $N = 3$, so $m \cdot n \cdot N^2 = 121\,500$ and $m \cdot N^3 = 6\,075$. Computational cost of (OCP_y) and (OCP_a) in Matlab–flops for one representative test are shown in Tab. 8.

No sophisticated algorithm was used for solving the second order system. In the example with $y_d = 150 \cdot \psi$, ψ from (23) and $\nu = 0.001$ (OCP_y) is solved after 4 SQP steps, while (OCP_a) needs 7 SQP steps. As stopping criterion for the algorithms the norm of the first order terms is required to be less then 10^{-6}.

Once the optimization problem (OCP_a) is solved and the optimal controls $b(t)$ and the state $a(t)$ are available, the function

$$u_b(t) := \sum b_j(t)\varphi_j$$

may serve as an suboptimal control for (1), or the pair (y_a, u_b) with

$$y_a(t) := \sum a_j(t)\varphi_j$$

as initial guess for the optimization problem (OCP_y).

We made some numerical tests comparing the cost $J(u_{opt})$ of problem (OCP_y) and $J(u_a)$ of problem (OCP_a) and, as we expected for our model problem the differences between them were small. We therefore omit the details. Instead we present the results for a different "suboptimal" approach, here called table steered feedback controller.

5.1 A table steered feedback controller

Let there be given an initial state a_0 and a stationary desired state a_d. Our aim is to steer the state $a(t)$ to a_d and wish to hold it there, even if perturbations occur. So we search for a feedback controller for that problem. Moreover, we assume to have available information on the position of the trajectory in the state space $\mathbb{R}^N$, even if perturbations occur. More precisely, we assume existence of a fixed, bounded domain $A \in \mathbb{R}^N$ such that $a(t) \in A$ for all t.
We choose a set of points α_k in A and attach a control $\beta_k \in \mathbb{R}^N$ to each of these points. Then a very simple feedback controller is given by

$$b(a(t)) = \beta_\kappa, \qquad \text{where} \quad \kappa = \arg\min_k \|a(t) - \alpha_k\|^2_{\mathbb{R}^N}. \tag{20}$$

So at each time t we look for the buoy α_k next to $a(t)$ and use the attached control β_k to correct our course. (Of course more sophisticated controllers make use of linear or spline interpolation instead of the piecewise constant Ansatz (20), see e.g. [8].)

To obtain the controls β_k we solve (OCP$_a$) subject to $a|_{t=0} = \alpha_k$ for every k. Then we set $\beta_k = b|_{t=0}$, where b is the optimal control for (OCP$_a$). (Another justification for that choice of β_k may be found in [8], [9], where a related approach is discussed.)
Obviously the quality of the feedback controller depends on the choice of the control horizon T for the subsidiary (OCP$_a$) problems (the larger we choose T the better we expect β_k to be) and from the choice of our navigation points α_k (the finer the grid of these points the better the controller).

From the tests of Section 4.2 we conclude that the first mode is the most important one for the dynamics of the POD system. This leads us to a design decision for the choice of the α_k. We ignore the coordinates of the second two modes in our grid, just taking into account the coordinate of the first mode:

$$\alpha_k = (s_k, 0, 0)^T. \tag{21}$$

So our grid of points will be managed as a simple table ordered with respect to the coordinate s_k of the first mode. We select a simple linear set of s_k as follows: With $\bar{s} := (a_d)_1$, $\partial s = |(a_d)_1 - (a_0)_1|$ and $K = 2L + 1$ we set

$$s_1 := \bar{s} - \partial s < s_2 := s_1 + \tfrac{\partial s}{L} < \cdots < s_{L+1} := \bar{s} < \cdots < s_K := \bar{s} + \partial s. \tag{22}$$

Note, that for this construction we have to assume that the desired state y_d is independent of time.

$\nu = 1$	(y,u)	$\|y - y_d\|_{L^2(Q)}$	$\|u\|_{L^2(Q)}$	$J(y,u)$
$y_d \equiv 1$	(y_{opt}, u_{opt})	$1.908348 \cdot 10^0$	$4.546876 \cdot 10^{-1}$	$1.924267 \cdot 10^0$
	(y_{tab}, u_{tab})	$1.907213 \cdot 10^0$	$4.628967 \cdot 10^{-1}$	$1.925868 \cdot 10^0$
$y_d \equiv 10$	(y_{opt}, u_{opt})	$2.619803 \cdot 10^1$	$1.069089 \cdot 10^1$	$4.003159 \cdot 10^2$
	(y_{tab}, u_{tab})	$2.686018 \cdot 10^1$	$1.114942 \cdot 10^1$	$4.228896 \cdot 10^2$
$y_d \equiv 100$	(y_{opt}, u_{opt})	$1.978790 \cdot 10^2$	$6.617176 \cdot 10^1$	$2.176740 \cdot 10^4$
	(y_{tab}, u_{tab})	$1.977076 \cdot 10^2$	$6.691062 \cdot 10^1$	$2.178267 \cdot 10^4$
$y_d \equiv 150$	(y_{opt}, u_{opt})	$3.464893 \cdot 10^2$	$1.320684 \cdot 10^2$	$6.874845 \cdot 10^4$
	(y_{tab}, u_{tab})	$3.454083 \cdot 10^2$	$1.361372 \cdot 10^2$	$6.892010 \cdot 10^4$

Table 9: Optimal controls compared to suboptimal table controls

5.2 Table gouverned control for (OCP_y)

Given an (OCP_y) we generate a table as described above for a_0 and a_d coordinates of the projections of y_0 and y_d onto span $\{\varphi_i\}$. Then we compute a suboptimal solution (y_{tab}, u_{tab}) with the following algorithm:

Algorithm 5.1 (Table gouverned control)

1. Given $y_{tab}(t)$ compute the coordinates with respect to the first mode: $\sigma = \langle y_{tab}(t), \varphi_1 \rangle$.
2. Determine the position between the neighboring buoys: Find $\vartheta \in [0,1]$ and $k \in \{1, \ldots, K-1\}$ such that $\sigma = \vartheta s_k + (1-\vartheta)s_{k+1}$.
3. Interpolate the attached controls $b = \vartheta\beta_k + (1-\vartheta)\beta_{k+1}$ and construct the actual suboptimal control $u_{tab}(t + \partial t) = \sum_{j=1}^{3} b_j \varphi_j$.
4. Compute the new state $y_{tab}(t+\partial t)$ using the semi implicit Euler scheme (6), update the time $t = t + \partial t$ and goto 1.

First we present results for some simple tests with $K = 21$. We observe a surprisingly good quality of the table optimizer. The little differences in cost between $J(y_{opt}, u_{opt})$ and $J(y_{tab}, u_{tab})$ in Tabs. 9, 10 in essence arise from the typical behaviour that an optimal control is weakened near the end of time T to reduce the cost of $\nu\|u\|^2$ at a time period when a little growing of $\|y - y_d\|^2$ has no longer much influence on the whole cost. However, the table controller is not designed to manage this last fine-tuning of the cost.

$\nu = 0.01$	(y,u)	$\|y - y_d\|_{L^2(Q)}$	$\|u\|_{L^2(Q)}$	$J(y,u)$
$y_d \equiv 1$	(y_{opt}, u_{opt})	$1.574401 \cdot 10^0$	$5.649420 \cdot 10^0$	$1.398950 \cdot 10^0$
	(y_{tab}, u_{tab})	$1.564106 \cdot 10^0$	$5.947244 \cdot 10^0$	$1.400062 \cdot 10^0$
$y_d \equiv 10$	(y_{opt}, u_{opt})	$1.604191 \cdot 10^1$	$8.007921 \cdot 10^1$	$1.607348 \cdot 10^2$
	(y_{tab}, u_{tab})	$1.591339 \cdot 10^1$	$8.301244 \cdot 10^1$	$1.610732 \cdot 10^2$
$y_d \equiv 100$	(y_{opt}, u_{opt})	$1.569158 \cdot 10^2$	$5.724924 \cdot 10^2$	$1.395002 \cdot 10^4$
	(y_{tab}, u_{tab})	$1.558275 \cdot 10^2$	$6.035232 \cdot 10^2$	$1.396230 \cdot 10^4$
$y_d \equiv 150$	(y_{opt}, u_{opt})	$2.370271 \cdot 10^2$	$9.662442 \cdot 10^2$	$3.275907 \cdot 10^4$
	(y_{tab}, u_{tab})	$2.355468 \cdot 10^2$	$1.004909 \cdot 10^3$	$3.279036 \cdot 10^4$

Table 10: Optimal controls compared to suboptimal table controls

After presenting the promising results above we next illuminate the limits of the control Algorithm 5.1 when it is applied to our test equation. Of course, the algorithm will not work very reliable for the control of unsymmetric desired states – but testing this seems to be not very fair. Remember that our controller just takes into account the projection of the state onto the first mode. It is much more natural to pose the question of how the feedback law performs in tracking states which are also composed of modes different to the first one. This motivates the following test with

$$\psi = \frac{\varphi_1 + \varphi_2}{\|\varphi_1 + \varphi_2\|_{L^\infty(\Omega)}} \approx$$

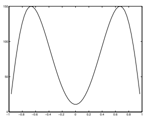

, (23)

whose results are presented in Tab. 11.

We observe that the table controller does not minimize the cost functional very good. But nevertheless it gives a useful control, which brings the state closer to the desired state than the optimal control does – probably due to the fact that the controller overestimates the distance between state and desired state, because of the poor information it has to rely on.
Nearly all these tests are made using $K = 21$ and $m = 225$, but with one exception. In order to avoid a massive overestimation of the growth of the state in the first small time phase which would lead to senseless results, for the case of $y_d = 100 \cdot \psi$ it is necessary to generate a table of $K = 41$ data sets using $m = 225$ time steps and then for computing u_{tab} to enlarge the number of time steps to $m = 450$.

	(y,u)	$\|y-y_d\|_{L^2(Q)}$	$\|u\|_{L^2(Q)}$	$J(y,u)$
$\nu = 0.001$				
$y_d = 1 \cdot \psi$	(y_{opt}, u_{opt})	$6.269820 \cdot 10^{-1}$	$2.786957 \cdot 10^{1}$	$5.849097 \cdot 10^{-1}$
	(y_{tab}, u_{tab})	$2.614458 \cdot 10^{-1}$	$4.045452 \cdot 10^{1}$	$8.524610 \cdot 10^{-1}$
$y_d = 10 \cdot \psi$	(y_{opt}, u_{opt})	$5.592994 \cdot 10^{0}$	$2.754180 \cdot 10^{2}$	$5.356832 \cdot 10^{1}$
	(y_{tab}, u_{tab})	$4.319824 \cdot 10^{0}$	$4.267563 \cdot 10^{2}$	$1.003909 \cdot 10^{2}$
$y_d = 100 \cdot \psi$	(y_{opt}, u_{opt})	$6.130370 \cdot 10^{1}$	$2.782969 \cdot 10^{3}$	$5.751532 \cdot 10^{3}$
	(y_{tab}, u_{tab})	$2.415023 \cdot 10^{1}$	$4.104272 \cdot 10^{3}$	$8.714142 \cdot 10^{3}$
$y_d = 150 \cdot \psi$	(y_{opt}, u_{opt})	$9.581969 \cdot 10^{1}$	$4.225719 \cdot 10^{3}$	$1.351906 \cdot 10^{4}$
	(y_{tab}, u_{tab})	$4.248790 \cdot 10^{1}$	$6.089232 \cdot 10^{3}$	$1.944198 \cdot 10^{4}$

Table 11: Numerical results for ψ given by (23)

	(y,u)	$\|y-y_d\|_{L^2(Q)}$	$\|u\|_{L^2(Q)}$	$J(y,u)$
$\nu = 0.001$				
$y_d = 1 \cdot \psi$	(y_{opt}, u_{opt})	$1.201466e+00$	$2.321152e+01$	$9.911473e-01$
	(y_{tab}, u_{tab})	$1.168352e+00$	$2.813463e+01$	$1.078302e+00$
$y_d = 10 \cdot \psi$	(y_{opt}, u_{opt})	$1.191781e+01$	$2.388593e+02$	$9.954403e+01$
	(y_{tab}, u_{tab})	$1.173236e+01$	$2.945266e+02$	$1.121971e+02$

Table 12: Numerical results for ψ given by (24)

A test with

$$\psi = \frac{\varphi_1 + \varphi_2 - \varphi_3}{\|\varphi_1 + \varphi_2 - \varphi_3\|_{L^\infty(\Omega)}} \approx \tag{24}$$

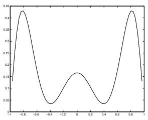

leads to similar results, see Tab. 12.

If we really want to make the table controller completely fail then we may use $\psi = 30 \cdot \varphi_2$, since $\frac{-\varepsilon^{-1}}{\min_x \varphi_2(x)} \approx 36.20$. Then the table just includes one entry according to $a_0 = 0$, which overestimates the control. So the state will be pushed below $-\varepsilon^{-1}$, which results in a numerical disaster.

5.3 Discussion of table controllers

The performance of the table controllers for the reduced Gelfand problem is very good. This partially seems to be due to the diffusive character of the equation. However, the numerical results for the Burgers equation with

Reynolds number Re= 100 presented in [9] indicate that this kind of feedback control also is applicable to problems with moderate transport.

In our current implementation it has to be avoided that the state is driven by the control beyond the borders of the grid. In order to be less restrictive in this case suitable extrapolation beyond the boarders of the grid should be provided. However, to make the table controller as reliable as possible the grid should be fine. This in turn necessitates a large amount of a-priori computations.

The most serious problem concerns state information. How can one get sufficient information on the state in order to obtain reasonable projections on the POD-modes? We suggest to seek for a best fit in the space spanned by the modes of the information on the state available. Furthermore, the incorporation of boundary control is a delicate issue.

5.4 Proper orthogonal decomposition for storage intensive problems

We point out another possibility to use POD in numerically solving optimal control problems like that given by (11). For large scale optimal control problems as they occur in fluid mechanics, say, besides computing power the most serious bottleneck is storage limitation. Due to the structure of time dependent control problems computing controls with an iterative algorithm in every iteration step at least necessitates the storage of the state, the adjoint variables and the controls on the whole time grid. Instead of this procedure we propose the following pseudo-code, where $G := \{t_0 < t_1 < \cdots < t_M\}$ denotes a fine grid and $G_S := \{s_0 < s_1 < \cdots < s_N\} \subset G$ $(N < M)$ denotes a coarser snapshot grid.

Algorithm 5.2 (POD replaces storage)

1. Compute the state y corresponding to the current control u on the fine time grid G. Save the snapshots $y(s_k)$ on the coarse grid G_S.

2. Compute POD modes according to the snapshots and solve the reduced state equation for $\tilde{y}$ on the fine grid G.

3. Compute the adjoint information λ on G with y replaced by $\tilde{y}$. Store snapshots of $\lambda(s_k)$ on G_S.

4. Compute the corresponding adjoint POD modes and and solve the reduced adjoint system for $\tilde{\lambda}$ on the fine grid G. The reduced adjoints on the fine grid are stored.

5. Update the control u on G using the adjoint information $\tilde{\lambda}$.

6. Goto 1.

A related approach to circumvent the storage problem in large-scale control problems involving the instationary Navier-Stokes equations is discussed by Berggren in [4]. There, the state information needed for the adjoint computations in the time interval $[s_i, s_{i+1}]$ is computed using the snapshot $y(s_i)$ as initial condition. Therefore, this method approximately doubles the amount of work necessary for numerically solving the optimal control problem. The additional numerical effort of Algorithm 5.2 is related to the number of snapshots used and thus marginal, at least if this number is small.

Clearly, controls computed with Algorithm 5.2 are not optimal. However, the quality of the controls can be estimated in terms of the approximation properties of the Rothe functions associated to the snapshots of the state and the adjoint information, respectively. For a more detailed discussion of this topic we refer to a subsequent paper.

6 Conclusions

The snapshot form of the proper orthogonal decomposition is used to compute approximate solutions and to develop suboptimal open- and closed-loop control strategies for the perturbed Gelfand equation.

The reduced system obtained by the POD-approximation resolves the dynamics of the original system very good. In most of the numerical examples 3 modes are sufficient for building the reduced dynamical system. This can be explained with the diffusive character of the perturbed Gelfand equation.

The behaviour of the reduced system is also investigated wrt perturbations of the external heating and the initial values. In order to resolve the dynamics of the perturbed system the snapshot set of the POD basis has to be modified in an appropriate way.

Several possibilities for using the reduced system for the computation of controls for the full system are worked out.

1. The optimal control of the reduced optimization problem may be used as initialisation in the optimization process of the full system.

2. A grid of controls build from the sensitivities which are computed from the optimization problems corresponding to the pairwise distinguish initial values on the grid is used to stabilize the full system.

3. Proper orthogonal decomposition can be used to reduce the storage requirements in the full optimization problem.

However, in general the quality of the suboptimal controls obtained by system reduction can not be quantified, except for the method proposed in point 3.

7 Epilogue: On the sense of numerical testing

Numerical testing is mostly an unpleasant job. If everything goes as expected it is boring and if things go wrong it may be frustrating to find out why. After testing it is sometimes not easy to present and explain the results. It is necessary to present tables of data to substantiate the ideas one concludes from test observations and make them somewhat checkable. Then one danger is to really bore the reader with too much tables of dead numbers, and another danger is not to be honest in the choice of data one wants to present, since there are nearly always more and less impressive results availiable. However we hope that You have taken a fancy to our exposition.

Acknowledgments

The authors acknowledge the support of the Sonderforschungsbereich 557 **Beeinflussung komplexer turbulenter Scherströmungen** located at the Technische Universität Berlin, Germany and sponsored by the **Deutsche Forschungsgemeinschaft** Furthermore, the first author acknowledges the support of a **Marie Curie Fellowship** sponsered by **European Union**.

References

[1] **Atwell, J.A.** & **King, B.B.** Proper Orthogonal Decomposition for reduced basis feedback controllers for parabolic equations. ICAM Report 99-01-01, 1999. Interdisciplinary Center for Applied Mathematics, Virginia Polytechnic Institute and State University Blacksburg, Virginia.

[2] **Aubry, N.** On the hidden beauty of the Proper Orthogonal Decomposition. *Theoret. Comput. Dynamics*, 2:339–352, 1991.

[3] **Bebernes, J.** & **Eberly, D.** *Mathematical Problems from Combustion Theory.* Springer, New York, 1989.

[4] **Berggren, M.** Numerical solution of a flow control problem: Vorticity reduction by dynamic boundary action. *Siam J. Sci. Comput.*, Vol. 19(No. 3), 1998.

[5] **Choi, H.; Hinze, M.** & **Kunisch, K.** Instantaneous control of backward-facing-step flows. Preprint No. 571/1997, 1997. Technische Universität Berlin, Deutschland.

[6] **Choi, H; Temam, R.; Moin, P.; Kim, J.** Feedback control for unsteady flow and its application to the stochastic Burgers equation. *J. Fluid Mech.*, 253:509 pp., 1993.

[7] **Hinze, M.** & **Kauffmann, A.** Control concepts for parabolic equations with an application to the control of fluid flow. Preprint No. 603/1998, 1998. Technische Universität Berlin, Deutschland, to appear in the Proceedings of the SCCE II, Hamburg Harburg.

[8] **Ito, K.** & **Kunisch, K.** Optimal control. Draft, 1998. Institut für Mathematik, Karl-Franzens Universität Graz, Austria.

[9] **Kunisch, K.** & **Volkwein, S.** Control of Burgers equation by a reduced order approach using Proper Orthogonal Decomposition. Bericht Nr. 138, Spezialforschungsbereich Optimierung und Kontrolle, September 1998.

[10] **Lee, C.; Kim, J.** & **Choi, H.** Suboptimal control of turbulent channel flow for drag reduction. *J. Fluid Mech.*, 358:245–258, 1998.

[11] **Sirovich, L.** Turbulence and the dynamics of coherent structures, Part I-III. *Quarterly of Applied Mathematics*, 45:561–590, 1987.

[12] **Tang, K.Y.; Graham, W.R.** & **Peraire, J.** Active Flow Control using a Reduced Order Model and Optimum Control. Preprint, 1996. Computational Aerospace Sciences Laboratory, MIT Department of Aeronautics and Astronautics.